Ground states of adsorbates on single-walled carbon nanotubes

Xiaobao Yang and Jun Ni
Department of Physics, Tsinghua University, Beijing 100084, People's Republic of China
(Received 25 November 2002; revised manuscript received 10 February 2003; published 6 May 2003)

We have investigated the ground states of single-walled carbon nanotubes with atoms adsorbed in the center of the hexagonal unit using the Monte Carlo method. We have determined the ground state structures of adsorbate on carbon nanotubes with different diameters. We have shown that the confinement has strong effects on the ground state structures. For the case of the zigzag $(n,0)$ nanotubes, when $n+1$ can be divided exactly by 6, the ground state structures is the same as those of planar triangular lattice. Otherwise, novel ground state structures are found as a result of the size confinement of the system. We have also compared the results of zigzag type structures with those of armchair type. It is shown that the rolling way influences the ground state structures.

DOI: 10.1103/PhysRevB.67.195403 PACS number(s): 68.43.De, 64.70.Nd, 61.46.+w, 05.50.+q

I. INTRODUCTION

Carbon nanotubes, as a promising new material, have important applications because of their unique physical, optical, and mechanical properties.[1–3] Adsorption on single-walled carbon nanotubes (SWNT's) is a subject of growing experimental and theoretical interest.[4–18] The adsorbate formed on carbon nanotubes have the potential of revolutionizing gas storage technology. The adsorption can be on individual SWNT and SWNT bundles.[11–18] The gas environment also affects the electronic conductance of both semiconducting and metallic nanotubes.[19–23]

A single-walled nanotube can be considered as a rolled graphite sheet. Extensive research has been carried out to investigate the interaction between graphite and adsorbate atoms.[24–28] The cluster model calculations have been used to study the positions of $3d$-transition metals adsorbed on graphite for three different sites.[27] It is found that the stable position of the V adatoms is on the center of the graphite hexagon and that the bridge and on-top sites are less stable.[27] For the rare gas monolayers with simple Lennard-Jones form interaction, the preferred adsorption sites for both krypton and xenon are the center of the graphite hexagon, whereas the least favorable is the one in which the rare gas atom is sitting directly on top of a carbon atom.[28] Two-dimensional rare gas solids exhibit remarkably rich and interesting behavior with new phenomena unique to two dimensions.[28–30] When the graphite is rolled into nanotubes, the center of each hexagonal unit are expected to be one of the preferred adsorption sites. For an individual SWNT, the first principle calculations of adsorption energy and the equilibrium positions show that the center of carbon hexagon are the optimal sites for gas molecule such as CO_2, H_2, N_2, and Ar.[18]

The triangular lattice gas model has been used to describe the behavior of submonolayers of adsorbate atoms on the graphite with center of carbon hexagon as adsorption sites.[31] The possible ground state spin configurations of an Ising model on a planar triangular lattice have been investigated using different methods.[32–34] The triangular lattice is a simple system exhibiting macroscopic ground state degeneracy due to the so-called frustration.[35] The frustration effect can be measured by frustration function defined on closed contours. When the graphite sheets is rolled into nanotubes, the system is confined in the rolling direction and new closed contours are formed along the the rolling direction which leads to an additional frustration effect in longer dimensions. The superimposition of this frustration effect due to confinement with the original frustration effects may result in new behaviors in the structures.

In this paper, we will study the ground state structures of adsorbate on individual SWNT's. The effects of the confinement on the ground state are analyzed. The changes of the ground states with the increase of the diameter of the nanotube are discussed. In Sec. II we describe the methods. Section III presents the results of the ground state structures of adsorbate on carbon nanotubes. Section IV is the summary.

II. METHODS

The structure of an individual carbon nanotube is specified in terms of a vector $\mathbf{C}$ joining two equivalent points on the original lattice. The nanotube is produced by rolling up the graphite sheet so that the two end points of the vector are superimposed. The vector $\mathbf{C}$ can be expressed as $\mathbf{C}=n\mathbf{a_1}+m\mathbf{a_2}$, thus each pair of integers (n,m) represents a possible tube structure.[1] In the following, we will consider the adsorption on the center of the carbon hexagon in a very long individual SWNT, for which the effects of two endings can be neglected. The adsorption is considered to be only on one side of [illegible] side of

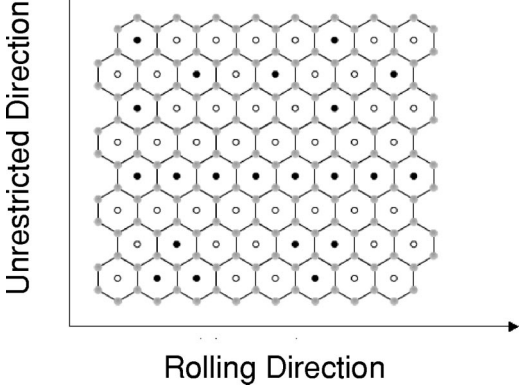

FIG. 1. Two unequivalent directions for the carbon nanotube: The rolling direction and the unrestricted direction.

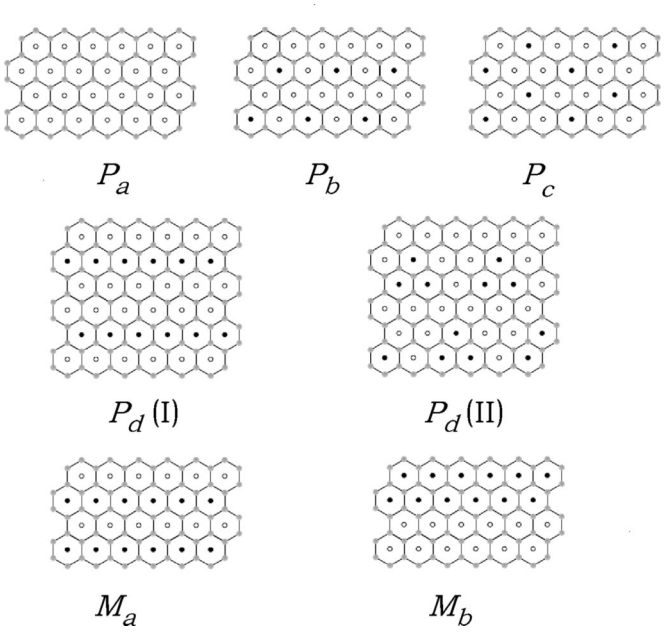

FIG. 2. The ground states for $n=5$ and planar triangular lattice. Gray circles represent carbon atoms, black circles represent adsorbed atoms, and white circles represent vacancies.

the nanotube. We first discuss the simplest case of $m=0$, which is zigzag type. We will also make a comparison with the case of armchair type with $m=n$. When the tube is unfolded as shown in Fig. 1, we can see that there are two inequivalent directions: the rolling direction and the unrestricted direction. The direction along the tube is unrestricted. The number of the carbon atoms in the rolling direction determines the diameter of the tube. From Fig. 1, we can see that the center sites of hexagonal unit form a triangular lattice.

In order to describe the possible structures of adsorbate on carbon nanotube, we use the Ising model. Under the Ising model, spin $s_i=1$ corresponds to atom occupying lattice site i, and $s_i=-1$ corresponds to vacancy occupying lattice site i. The interactions between adsorbed atoms and carbon nanotube are same for all sites and can be described by the chemical potential. The Hamiltonian is given as

$$\mathcal{H}=J_1\sum_{NN} s_i s_j + J_2\sum_{NNN} s_i s_j + \mu\sum_i s_i, \qquad (1)$$

where J_1 is the nearest-neighbor interaction, J_2 is the next nearest-neighbor interaction, and μ is the chemical potential. The first sum runs over all the nearest-neighbor atom pairs, the second sum runs over all the next nearest-neighbor atom pairs, and the last sum runs over all the sites. The energy per site corresponding to Eq. (1) can be written as

$$\mathcal{H}/N=c_1J_1+c_2J_2+m\mu. \qquad (2)$$

The relative Ising magnetization m is restricted to the range $[-1,1]$ and the average spin correlations c_1 and c_2 are restricted to $[-3,3]$.

We use Monte Carlo simulation to get all the possible ground states of the system.[36,37] In the calculation, we allow the system to anneal down from a state at high temperature to the state at low temperature. During the process of annealing, a spin flipping mechanism is used to get the configuration with minimal free energy. When temperature approaches zero, the system will be annealed into the ground state. In order to obtain all possible ground states we scan the parameters space of chemical potential and interaction energy. Since $|J_1|$ can be considered as a renormalized parameter, we consider only the parameter space of μ and J_2. In each annealing process, we select different μ in the step of 0.2 from -10 to 10 and different J_2 in the step of 0.05 from -2 to 2. When the triangular lattice in a geometry plane is rolled to form the tube, one direction is confined. $n+1$ corresponds to the number of the adsorption sites on the carbon nanotube in the rolling direction. For the carbon nanotubes of zigzag type, the smallest n of nanotubes grown by experiments is 5.[38] The length of the carbon nanotubes is described by the number l, which will be taken large enough for ending effects to be neglected. We take $l=60$ and use the periodic boundary condition. The calculations on other geometries such as $l=80$ and $l=120$ are also performed and the same results are obtained. In order to find how the ground states changes as the size increases, we have calculated different diameters with n beginning from 5.

III. RESULTS

When the diameter of nanotube approaches infinite, it become the case of planar triangular lattice. The possible

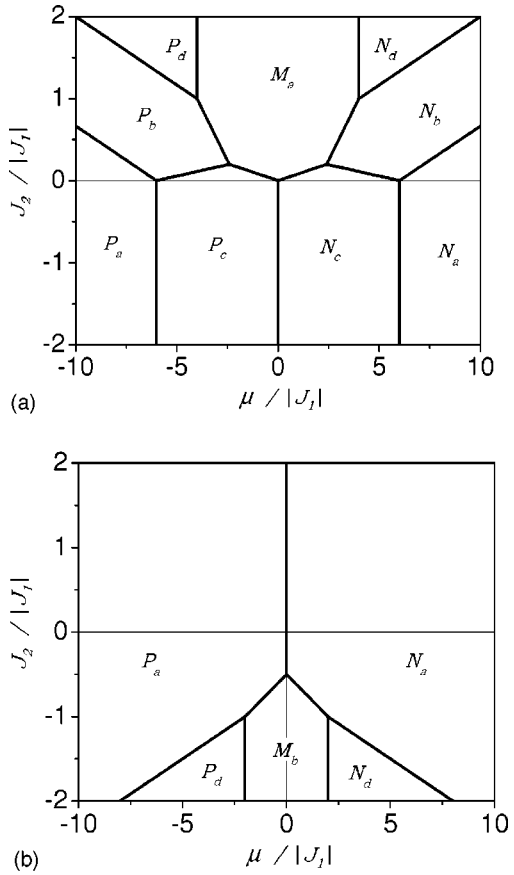

FIG. 3. The ground state phase diagram for the case of $n=5$. (a) $J_1>0$; (b) $J_1<0$.

TABLE I. The ground states for the case of zigzag type $(n,0)$ nanotubes $(n \geqslant 5)$.

n	Phase No.	c_1	c_2	m	Structure
any	P_a	3	3	1	$(n+1)\times A$
$n=2k-1$	P_b	0	0	1/2	$k\times B$
$n=2k+2$	P_{b1}	$3/(n+1)$	$3/(n+1)$	$(n+2)/2(n+1)$	$k\times B+B_a$
	P_{b2}	$1/(n+1)$	0	1/2	$k\times B+B_b$
	P_{b3}	$-1/(n+1)$	$-1/(n+1)$	$n/2(n+1)$	$k\times B+B_c$
	P_{b4}	0	$6/(n+1)$	1/2	$k\times B+B_d$
$n=3k-1$	P_c	-1	3	1/3	$k\times C$
$n=3k+3$	P_{c1}	$-1+4/(n+1)$	$3-4/(n+1)$	$1/3+2/3(n+1)$	$k\times C+C_a$
	P_{c2}	$-1+4/(n+1)$	$3-8/(n+1)$	$1/3+2/3(n+1)$	$k\times C+C_b$
	P_{c3}	-1	$3-4/(n+1)$	$1/3-1/3(n+1)$	$k\times C+C_c$
$n=3k+4$	P_{c4}	$-1+2/(n+1)$	$3-4/(n+1)$	$1/3+1/3(n+1)$	$k\times C+C_d$
	P_{c5}	-1	$3-8/(n+1)$	$1/3-2/3(n+1)$	$k\times C+C_e$
	P_{c6}	-1	$3-4/(n+1)$	$1/3-2/3(n+1)$	$k\times C+C_f$
	P_{c7}	$-1+1/(n+1)$	$3-7/(n+1)$	$1/3-1/6(n+1)$	$k\times C+C_g$
any	P_d	1/3	-1	1/3	$(n+1)\times D_{\mathrm{I}}$ [a]
any	M_a	-1	-1	0	$(n+1)\times E$
any	M_b	1	-1	0	$(n+1)\times F$

[a]When $n+1$ can be divided exactly by 3, there is another energy-degenerated ground state structure $(n+1)/3\times D_{\mathrm{II}}$ for P_d.

ground state structures on a planar triangular lattice have been found by the inequality method.[32–34] There are ten possible ground states. Two of them have degenerate structures. In the following, we will show that when $n+1$ can be divided exactly by 6, the ground state structures is the same as those of planar triangular lattice. The possible ground state ordered structures are shown in Fig. 2. In the figure, the structures containing more vacancies are named using characters beginning with P(P stands for ''positive'' to represent the case when the number of $s_i=1$ is larger than that of $s_i=-1$) while those with fewer vacancies are named using characters beginning with N(N stands for ''negative'' to represent the case when the number of $s_i=-1$ is larger than that of $s_i=1$). Those containing equal number of atoms and vacancies are named using characters beginning with M(M stands for ''middle''). Roman characters such as I, II are used to distinguish degenerated structures. The structures with character N are counterparts of those with character P by exchanging atoms with vacancies. The only difference of the energy expressions for these two types of structures is that the signs of the chemical potential for them are opposite. In order to show how the ordered ground states change with the chemical potential,[39] we display the ground state phase diagrams in Fig. 3. The ground state phase diagrams shown in Fig. 3 have a mirror symmetry in the structure distribution perpendicular to the axis of chemical potential. Thus, we need only to discuss the structures beginning with P and M. In the following, we will focus on how the structures change as the diameter of the nanotube increases.

Now we discuss the case of $n=5$ which corresponds to the carbon nanotube with the smallest diameter grown by experiments.[38] The results show that it has the same ground states as planar triangular lattice. The reason is as follows. From Fig. 2, it can be seen that for a planar triangular lattice, the ground state structures have periodicity of two, four and six adsorption sites in the unrestricted direction and periodicity of one, two, and three adsorption sites in the rolling direction. If the number $n+1$ of adsorption sites in the rolling direction can be divided by 6 exactly, the types of ground state will be the same as those of the planar triangular lattice because the ground state structures for the planar triangular lattice has periodicity of one, two, and three adsorption sites. Otherwise, new ground state structures will be derived due to

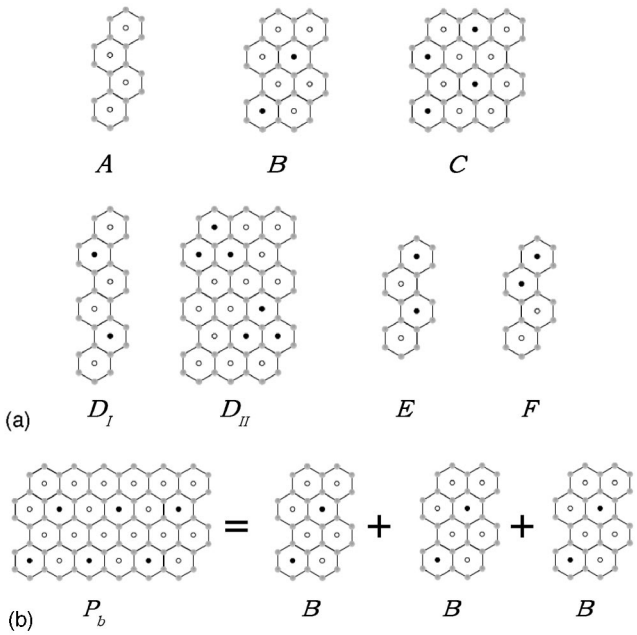

FIG. 4. (a) The basic substructures selected to describe the ground state structures. (b) Representation of the ground state structure P_b by three basic substructures BBB.

the confinement in the rolling direction. Therefore, there are ten possible ground states, two of which have degenerate structures. The simulations gives the same results as the above analysis. All the possible ground state structures are the same as those for the case of planar triangular lattice as shown in Fig. 2. The phase diagrams of ground state are shown in Fig. 3. We select basic substructures shown in Fig. 4(a) to describe the ground states for convenience. For example, the structure P_b can be represented by BBB as illuminated in Fig. 4(b). We use integers such as 1, 2 to mark the structures derived as a result of the confinement of system. The energies of all the ground state structures obtained are shown in the Table I. Table I also shows how to form ground state structures with basic and derived substructures.

When $n+1$ can be divided by the site number of basic substructures along the rolling direction, there are no new ground state structures and the phase diagram will not break up. Otherwise, it will be in contradiction to the results for planar triangular lattice. For the case of $J_1<0$, the site number of basic substructures along the rolling direction is one. Thus nanotubes for all diameters should have the same ground state structures with the triangular plane lattice, which are also confirmed by our results of the Monte Carlo simulations. In the following, we will only focus on the case of $J_1>0$.

The case of $n=6$ is much more complicated because $n+1=7$ can not be divided exactly either by 2 or by 3. New ground state structures have been found to replace the structures P_b and P_c. We find that there are four new ground state structures derived from the structures P_b, all of which have similar characteristic in structures. There are also four new ground state structures for N_b, which is counterpart of P_b by exchanging atoms with vacancies. As is shown in Fig. 5, there are four new derived substructures together with basic substructures to describe the ground state structures. Figure 5 also shows how to form structures with basic and derived substructures. The basic substructure B combines with the derived substructures to form the ground state structures. The derived substructures can be considered as a transitionary region due to the confinement along the rolling direction. The derived substructure B_d looks more similar to the basic substructure C. Thus it is comprehensible that this structure is found near the boundary region of ground state structures P_b and P_c in the ground state phase diagram shown in Fig. 6. There are three new ground state structures derived from the structures P_c and three for N_c. We can introduce three new derived substructures shown in Fig. 5 together with basic substructures to describe the ground state structures. From the phase diagram of the ground states shown in Fig. 3(a), the area occupied by P_b in the case of $n=5$ has been divided into four subregions for the four new ground state structures, which is shown in Fig. 6. The total area has been reduced because the derived structures have higher energies. The number of the ground states for the case of $n=6$ is 20 , eight of which are derived from the ground state structures P_b and N_b, six of which are derived from the ground state structures P_c and N_c.

When $n=7$, no new ground state structures are derived from the ground state structure P_b because $n+1=8$ can be divided exactly by 2. But $n+1$ cannot be divided exactly by 3, thus other ground state structures are found. When divided by three, seven and eight have different remainders. Thus the derived substructures from P_c for $n=7$ as shown in Fig. 7 are different than those for $n=6$. The ways that the phase diagrams of the ground states break up are also different. The number of the ground states for $n=7$ is 16, eight of which are derived from the ground state structures P_c and N_c.

As the number n changes from eight to ten, we can see the similar variation. When $n=8$, no new ground state structures are derived from P_c. The new ground state structures derived from P_b are similar to the ones of $n=6$, and the derived substructures are the same as those of $n=6$. The number of the ground states is 16, eight of which are derived

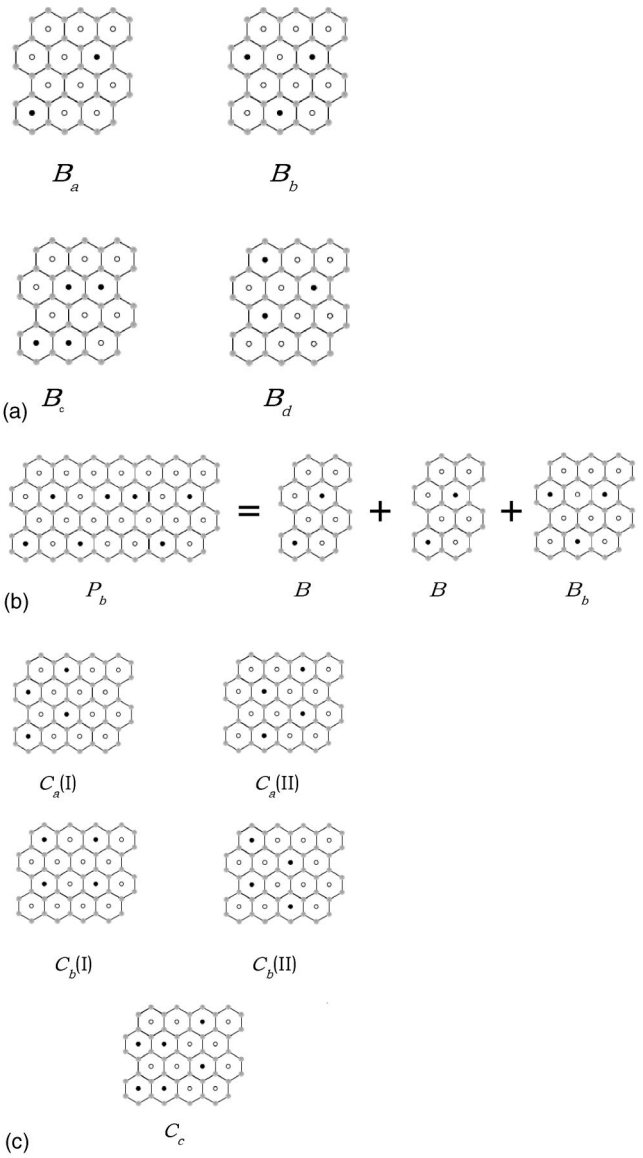

FIG. 5. The derived substructures for the case of $n=6$. The energetically degenerated ones are distinguished by Roman characters such as I, II. (a) The derived substructures selected to describe the ground state structure P_{bi}. (b) Representation of the ground state structure P_{b2} by three substructures BBB_b. (c) The derived substructures selected to describe the ground state structure P_{ci}.

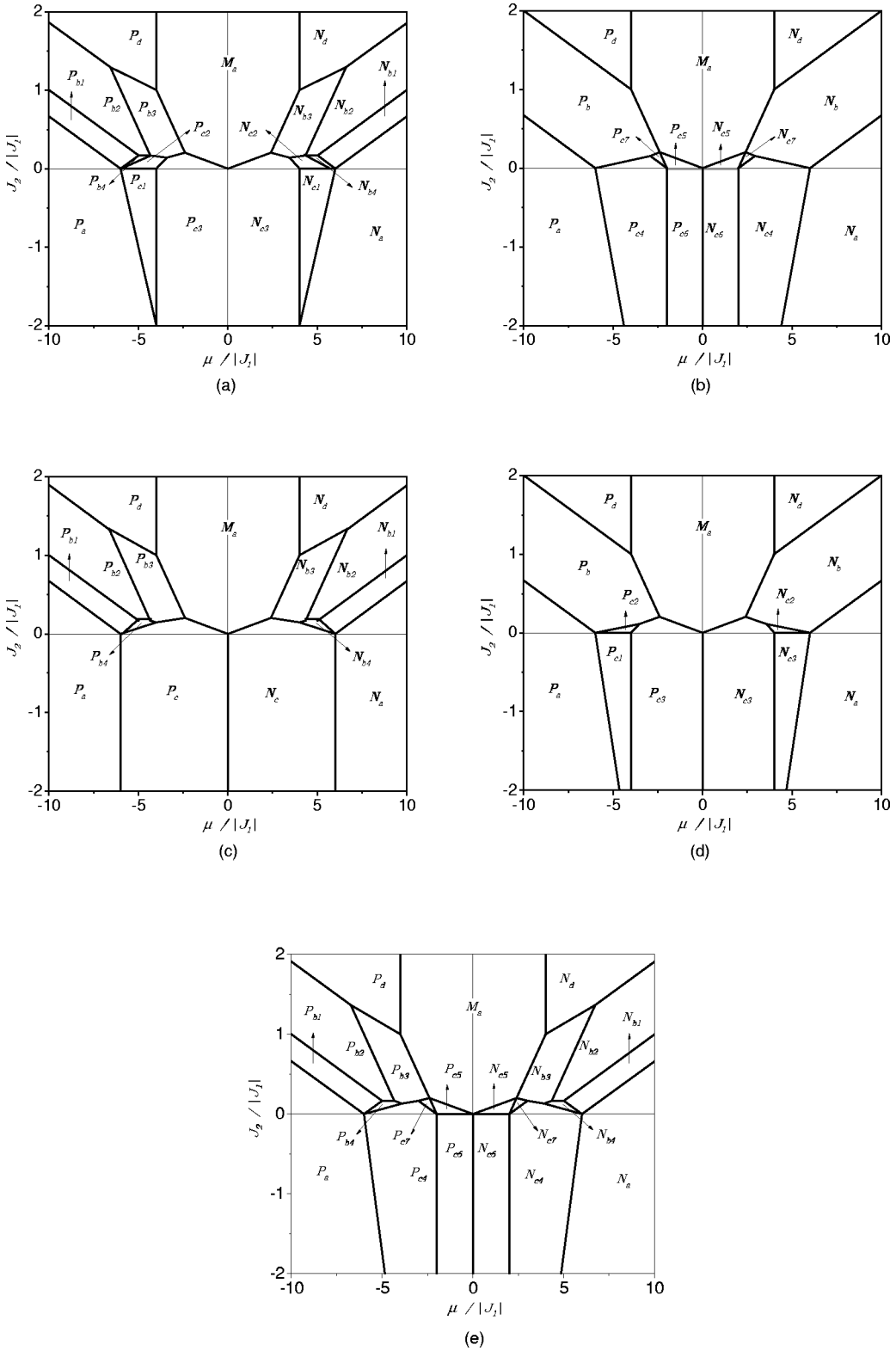

FIG. 6. The ground state phase diagram (a) for the case of $n=6$; (b) for the case of $n=7$; (c) for the case of $n=8$; (d) for the case of $n=9$; (e) for the case of $n=10$.

from the ground state structures P_b and N_b. When $n=9$, no new ground state structures are derived from P_b. The new ground state structures derived from P_c are similar to those of $n=6$ and the derived substructures are the same as those of $n=6$. The number of the ground states is 14, six of which are derived from the ground state structures P_c and N_c. When $n=10$, the new ground state structures derived from P_c are similar to those of $n=6$ and the derived substructures

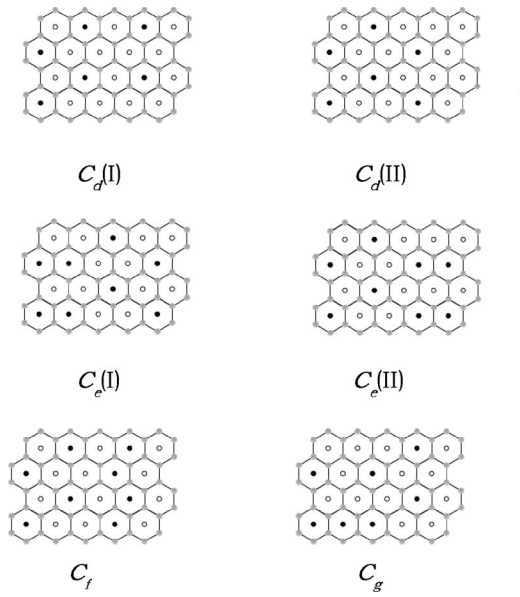

FIG. 7. The new derived substructures for the case of $n=7$. The energetically degenerated ones are distinguished by Roman characters such as I, II.

are the same as those of $n=6$. The new ground state structures derived from P_b are similar to those of $n=6$ and the derived substructures are the same as those of $n=6$. The number of the ground states is 22, among which eight are derived from P_b and N_b and eight are derived from P_c and N_c. When $n=11$, the case is the same as that of $n=5$ and the case of $n=12$ should be the same as that of $n=6$. Figure 6 shows the ground state phase diagrams for n changing from six to ten. From the phase diagram of the ground states, the area occupied by P_b in Fig. 3(a) is divided into four subregions for the cases of $n+1=7,9,11$ in similar ways, because these numbers have the same remainders when divided by 2. The area occupied by P_c is divided into three subregions for the cases of $n+1=7,10$ in similar ways, because these numbers have the same remainders when divided by 3. For the cases of $n+1=8,11$, the area occupied by P_c is divided into four subregions in the similar ways because these numbers have the same remainders when divided by

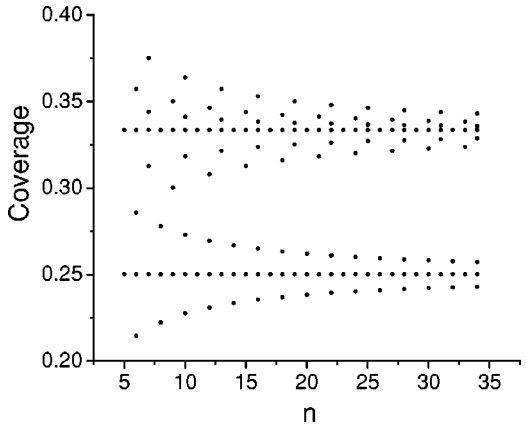

FIG. 8. The variation of the coverage as a function of n.

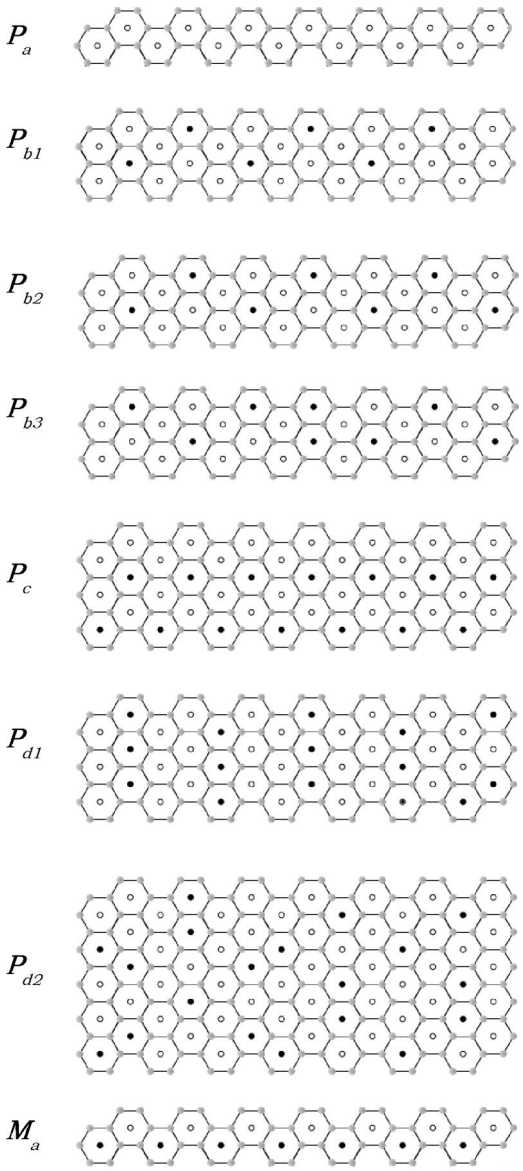

FIG. 9. Ground state structures obtained for armchair-type (7,7) nanotubes for $J_1>0$.

three. For those $n+1$ with the same remainder when $n+1$ is divided by 6, the ground state phase diagrams are similar. We have deduced the ground state structures for different n's from our simulation results and we have shown the ground state structures described with basic and derived substructures in Table I. The energies per site for all ground state structures are also shown in Table I.

The number of the ground states has a periodicity of 6. If n cannot be divided exactly by 2, 6 will be added to the number of the ground states. If n cannot be divided exactly by 3, 4, or 6 will be added to the number of the ground states depending on the remainder is 1 or 2. Thus the number of the ground states will depend on the remainder of $n+1$ divided by 6. Figure 8 shows that the coverage changes with the number of n. The derived structures have different coverages than the basic substructures, which leads to the change of coverage with n. As the number n increases, the derived sub-

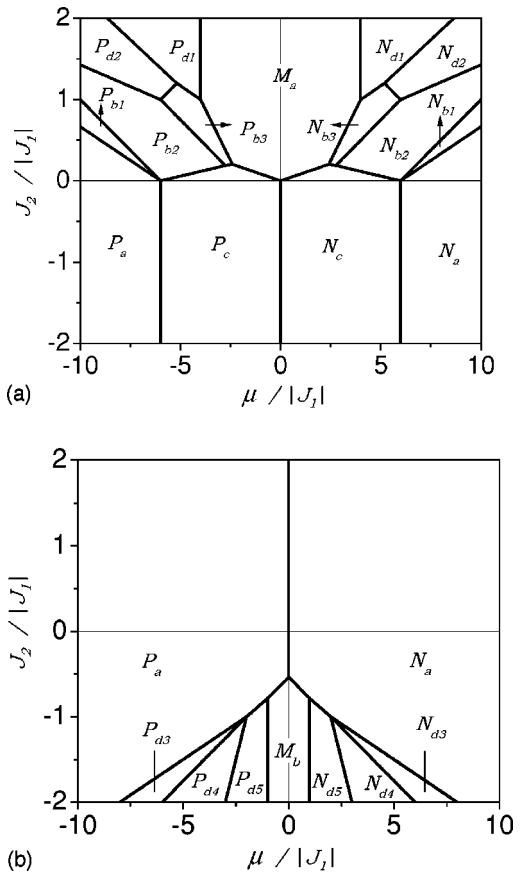

FIG. 10. The ground state phase diagram for armchair-type (7,7) nanotubes. (a) $J_1>0$, (b) $J_1<0$.

structures play a less important role and will approach the case of a planar triangular lattice.

In order to find the relationship between the ground state structures and the rolling type of carbon nanotubes, we have made calculations on the armchair type nanotubes with different diameters. There are new ground state structures for P_b and P_d because the basic substructure for P_b has periodicity of two adsorption sites and the basic substructure for P_d has periodicity of three adsorption sites. In the case of zigzag type $(n,0)$, we find that the sizes of the derived substructures are larger than the basic substructures and the derived substructures have local structural similarity with the basic substructures. In the case of armchair-type (n,n) nanotubes the derived structures are more complicated. n corresponds to the number of the adsorption sites on carbon nanotubes in the rolling direction. When n cannot be divided by 6 exactly, there are new ground states with complicated structures. We have compared the results for the zigzag (6,0) nanotubes with those for the armchair (7,7) nanotubes to show how the rolling type influences the ground state structures. The ground state structures and the phase diagram of ground states for the armchair (7,7) nanotubes for $J_1>0$ are shown in Figs. 9 and 10(a). In the case of the zigzag (6,0) nanotubes, derived structures are found for P_b and P_c because $n+1=7$ cannot be divided exactly either by 2 or by 3. The regions in the ground state phase diagram for P_b and P_c break up into four and three subregions, respectively. In the case of the armchair (7,7) nanotubes, there are derived structures for P_b and P_d because $n=7$ cannot be divided exactly either by 2 or by 3. Thus the region in the ground state phase diagram breaks up into three and two subregions, respectively, as shown in Fig. 10(a). For the structures derived from P_b, P_{b1}, P_{b2}, and P_{b3} for the armchair (7,7) nanotubes are similar to those for the zigzag (6,0) nanotubes, and the energies for the corresponding structures are also similar, as is shown in Table II. We cannot find the corresponding structure to P_{b4} of the zigzag (6,0) nanotubes. This is reasonable because P_{b4} is a kind of transitionary structure for P_b and P_c. In the case of the armchair (7,7) nanotubes, no new ground state structures are derived from P_c, thus P_{b4} should not exist for armchair-type (7,7) nanotubes. In the case of the zigzag (6,0) nanotubes, no new ground state structures are found from P_d because the basic substructure has periodicity of one adsorption site. In the case of the armchair (7,7) nanotubes, P_{d2} is found near the boundary region of the ground state structures P_b and P_d in the phase diagram of ground states. When $J_1<0$, new ground state structures are found from P_d. The phase diagram of ground states is shown in Fig. 10(b), and the ground state structures are shown in Fig. 11. From the above analysis, it can be seen that the rolling type has strong effects on the ground state structures.

TABLE II. Comparison of the ground states between the zigzag-type (6,0) nanotubes and the armchair-type (7,7) nanotubes.

Zigzag (6,0) type				Armchair (7,7) type			
Phase No.	c_1	c_2	m	Phase No.	c_1	c_2	m
P_a	3	3	1	P_a	3	3	1
P_{b1}	3/7	3/7	4/7				
P_{b2}	1/7	0	1/2	P_{b1}	3/7	3/7	4/7
P_{b3}	$-1/7$	$-1/7$	3/7	P_{b2}	0	1/7	1/2
P_{b4}	0	6/7	1/2	P_{b3}	$-1/7$	$-1/7$	3/7
P_{c1}	$-3/7$	17/7	3/7				
P_{c2}	$-3/7$	13/7	3/7	P_c	-1	3	1/3
P_{c3}	-1	17/7	2/7				
				P_{d1}	1/7	-1	2/7
				P_{d2}	1/7	$-9/35$	16/35
P_d	1/3	-1	1/3	P_{d3}	5/7	$-3/7$	3/7
				P_{d4}	11/21	$-17/21$	1/3
				P_{d5}	5/7	-1	1/7
M_a	-1	-1	0	M_a	-1	-1	0
M_b	1	-1	0	M_b	6/7	-1	0

IV. SUMMARY

We have investigated the ground states of adsorbate on individual single-walled carbon nanotubes. We have found that the ground state structures change as the diameter of the carbon nanotubes increases and determined the ground state structures for different diameters of carbon nanotubes. From the results and analysis shown above, we can see that the

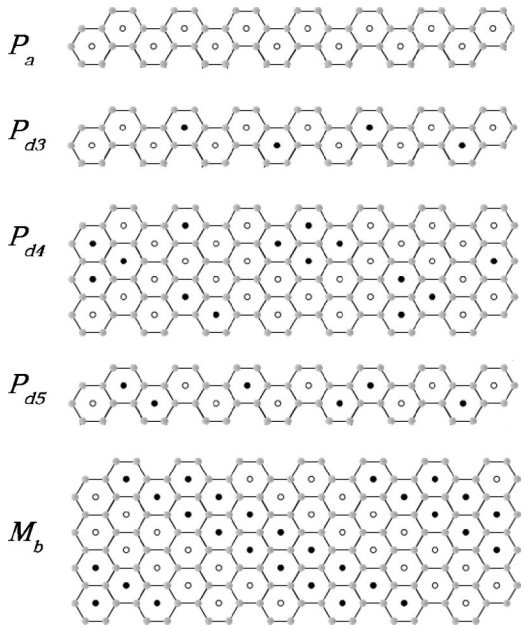

FIG. 11. Ground state structures obtained for armchair-type (7,7) nanotubes for $J_1<0$.

confinement has strong effects on the ground state structures. When $n+1$ can be divided exactly by six, the ground state structures for the zigzag-type carbon nanotubes are the same as those of the planar triangular lattice. Otherwise, new ground state structures are found as a result of the size confinement of the system. If $n+1$ cannot be divided exactly by 2, there are eight new ground states. If $n+1$ cannot be divided exactly by 3, there are six and eight new ground states, respectively, depending on the remainder being 1 or 2.

We can use the basic substructures and the derived substructures to describe the ground states. It is found that the sizes of the derived substructures are generally larger than those of the basic substructures. The derived structures have higher energies. In order to maintain the lowest energy state for the ground states, the structures should contain as many basic substructures as possible. For the basic substructures in the case of zigzag type nanotubes, periodicity of n for the ground states is six and the results are in agreement with our predictions. When the carbon nanotubes is rolled up in the way of armchair type, the case is more complicated and the derived substructures for the new ground state structures depend on the number n. As the number n increases, the derived substructures play less important role and it will approach to the case of planar triangular lattice. In addition to the adsorption on the center of carbon hexagon, the top site can also be the preferred adsorption site for some types of atoms and molecules. It forms a hexagonal lattice. The planar hexagonal lattice has an infinite series of ground states[40] and the case should become more complicated as a result of the confinement.

ACKNOWLEDGMENTS

This research was supported by National Key Program of Basic Research Development of China (Grant No. G2000067107) and the National Natural Science Foundation of China under Grant No. 10274036.

[1] P. J. F. Harris, *Carbon Nanotubes and Related Structures* (Cambridge University Press, London, 1999).
[2] M. S. Dresselhaus, *Carbon Nanotubes* (Springer, Berlin, 2001).
[3] H. J. Dai, Surf. Sci. **500**, 218 (2002).
[4] M. S. Dresselhause, K. A. Williams, and P. C. Eklund, MRS Bull. **24**, 45 (1999).
[5] A. C. Dillon, K. M. Jones, T. A. Bekkedahl, C. H. Kiang, D. S. Bethune, and M. L. Heben, Nature (London) **386**, 377 (1997).
[6] S. Inoue, N. Ichikuni, T. Suzuki, T. Uematsu, and K. Kaneko, J. Phys. Chem. B **102**, 4689 (1998).
[7] W. Teizer, R. B. Hallock, E. Dujardin, and T. W. Ebbesen, Phys. Rev. Lett. **82**, 5305 (1999).
[8] P. Chen, X. Wu, J. Lin, and K. L. Tan, Science **285**, 91 (1999).
[9] Y. Ye, C. C. Ahn, C. Witham, B. Fultz, J. Liu, A. G. Rinzler, D. Colbort, K. A. Smith, and R. E. Smalley, Appl. Phys. Lett. **74**, 2307 (1999).
[10] Q. Wang, S. R. Challa, D. S. Sholl, and J. K. Johnson, Phys. Rev. Lett. **82**, 956 (1999).
[11] G. Stan, M. J. Bojan, S. Curtarolo, S. M. Gatica, and M. W. Cole, Phys. Rev. B **62**, 2173 (2000).
[12] S. E. Weber, S. Talapatra, C. Journet, A. Zambano, and A. D. Migone, Phys. Rev. B **61**, 13 150 (2000).
[13] S. Talapatra, A. Z. Zambano, S. E. Weber, and A. D. Migone, Phys. Rev. Lett. **85**, 138 (2000).
[14] A. J. Zambano, S. Talapatra, and A. D. Migone, Phys. Rev. B **64**, 075415 (2001).
[15] M. M. Calbi, M. W. Cole, S. M. Gatica, M. J. Bojan, and G. Stan, Rev. Mod. Phys. **73**, 857 (2001).
[16] K. A. Williams, B. K. Pradhan, P. C. Eklund, M. K. Kostov, and M. W. Cole, Phys. Rev. Lett. **88**, 165502 (2002).
[17] H. Ulbricht, G. Moos, and T. Hertel, Phys. Rev. B **66**, 075404 (2002).
[18] J. J. Zhao, A. Buldum, J. Han, and J. P. Lu, Nanotechnology **13**, 195 (2002).
[19] J. Kong, N. R. Franklin, C. Zhou, M. G. Chapline, S. Peng, K. Cho, and H. J. Dai, Science **287**, 622 (2000).
[20] P. G. Collins, K. Bradley, M. Ishigami, and A. Zettl, Science **287**, 1801 (2000).
[21] X. P. Tang, A. Kleinhammes, H. Shimoda, L. Fleming, K. Y. Bennoune, S. Sinha, C. Bower, O. Zhao, and Y. Wu, Science **288**, 492 (2000).
[22] G. U. Sumanasekera, C. Adu, S. Fang, and P. C. Eklund, Phys. Rev. Lett. **85**, 1096 (2000).
[23] S. H. Jhi, S. G. Louie, and M. L. Cohen, Phys. Rev. Lett. **85**, 1710 (2000).
[24] G. Vidali, G. Ihm, H. Y. Kim, and M. W. Cole, Surf. Sci. Rep. **12**, 133 (1991).
[25] M. S. Dresselhaus and G. Dresselhaus, Adv. Phys. **30**, 139 (1981).
[26] M. Endo and M. S. Dresselhaus, Carbon **37**, 561 (1999).

[27] P. Kruger, J. C. Parlebas, and A. Kotani, Phys. Rev. B **59**, 15093 (1999); P. Kruger, M. Taguchi, J. C. Parlebas, and A. Kotani, *ibid.* **55**, 16 466 (1997).
[28] R. J. Birgeneau and P. M. Horn, Science **232**, 329 (1986).
[29] B. Joos, B. Bergersen, and M. L. Klein, Phys. Rev. B **28**, 7219 (1983).
[30] B. Joos and M. S. Duesbery, Phys. Rev. B **33**, 8632 (1986).
[31] B. Mihura and D. P. Landau, Phys. Rev. Lett. **38**, 977 (1977).
[32] U. Brandt and J. Stolze, Z. Phys. B: Condens. Matter **64**, 481 (1986).
[33] M. Kaburagi and J. Kanamori, Jpn. J. Appl. Phys., Suppl. **2**, 145 (1974).
[34] J. Kanamori, Ann. Phys. (Paris) **10**, 43 (1985).
[35] G. Toulouse, Commun. Phys. (London) **2**, 115 (1977).
[36] D. P. Landau and K. Binder, *A Guide to Monte Carlo Simulations in Statistical Physics* (Cambridge University Press, Cambridge, 2000).
[37] H. Liu, J. Ni, and B. L. Gu, Eur. Phys. J. B **26**, 261 (2002).
[38] L. C. Qin, X. L. Zhao, K. Hirahara, Y. Miyamoto, Y. Ando, and S. L. Ijima, Nature (London) **408**, 2 (2000).
[39] J. Ni and S. Iwata, Phys. Rev. B **52**, 3214 (1995).
[40] J. Kanamori, J. Phys. Soc. Jpn. **53**, 250 (1984).